Dalton Transactions

ROYAL SOCIETY OF CHEMISTRY

PAPER

View Article Online
View Journal | View Issue



Check for updates

Cite this: *Dalton Trans.*, 2024, **53**, 9042

# Crystal-to-crystal polymerisation of monosubstituted $[PW_{11}O_{39}Cu(H_2O)]^{5-}$ Keggin-type anions†

Estibaliz Ruiz-Bilbao, [a,b] Aroa Pache,[a] Unai Barrenechea,[a] Santiago Reinoso, [c] Leire San Felices, [d] Maria dM. Vivanco, [e] Luis Lezama, [a] Beñat Artetxe *[a] and Juan M. Gutiérrez-Zorrilla *[a,b]

The reaction between neutral bis(picolinate)copper(II) complexes and copper(II)-monosubstituted Keggin-type phosphotungstate anions formed *in situ* leads to the formation of the hybrid $[C(NH_2)_3]_{10}[\{PW_{11}O_{39}Cu(H_2O)\}_2\{Cu(pic)_2\}]\cdot 10H_2O$ compound (**1**, pic = picolinate) in the presence of structure-directing guanidinium cations. Single-crystal X-ray diffraction studies demonstrate that **1** contains dimeric $\{PW_{11}O_{39}Cu(H_2O)\}_2\{Cu(pic)_2\}$ molecular species constituted by two Keggin-type anions linked by one $\{Cu(pic)_2\}$ octahedral complex through axial coordination to their terminal oxygen atoms. The extensive hydrogen-bonding network established by guanidium cations and Keggin clusters plays a key role in retaining the crystallinity of the system throughout dehydration to allow a single-crystal-to-single-crystal (SCSC) transformation into the anhydrous $[C(NH_2)_3]_{10}[\{PW_{11}O_{39}Cu\}_2\{Cu(pic)_2\}]$ (**2a**) at 170 °C. Structural modifications involve the re-orientation, shifting in *ca.* 1.5 Å and condensation of all the $\{PW_{11}O_{39}Cu\}$ units to result in $\{PW_{11}O_{39}Cu\}_n$ chains in an unprecedented solid-state polymerisation. This phase transition also implies the cleavage of Cu–O bonds induced by the rotation and translation of Keggin-type anions, in such a way that hybrid dimeric units in **1** are dismantled and $\{Cu(pic)_2\}$ complexes become square planar. The irreversibility of the phase transition has been confirmed by combined thermal and diffractometric analyses, which evidence that the anhydrous phase adsorbs only one water molecule per cluster to become the $[C(NH_2)_3]_{10}[\{PW_{11}O_{39}Cu\}_2\{Cu(pic)_2\}]\cdot 2H_2O$ (**2h**) hydrated derivative without any significant alteration in its cell parameters, nor in its crystalline structure. Phase transformations have been monitored by electron paramagnetic resonance spectroscopy.

Received 7th March 2024,
Accepted 7th May 2024

DOI: 10.1039/d4dt00690a

rsc.li/dalton

## Introduction

Smart materials with bulk properties that can be tuned (*e.g.* magnetic, luminescent, catalytic, conductive, adsorptive) upon the application of an external stimulus, such as heat, pressure, light, or the presence of chemical species, have long been object of study.[1–5] In particular, the interest on the occurrence of single-crystal-to-single crystal (SCSC) transformations lies on the possibility to monitor how the specific location of the atoms varies, which allows to correlate structural changes with variations in the final properties. In the best-case scenario, fine control of the applied stimulus could adjust the response of the materials, paving the way for the construction of practical tools, such as molecular switches, sensors or storing devices.[6,7]

Although several coordination compounds that can undergo SCSC transformations can be nowadays found in the literature,[8–10] incorporation of rigid building blocks within the framework could systematically help to prevent structural col-

[a]*Departamento de Química Orgánica e Inorgánica, Facultad de Ciencia y Tecnología, Universidad del País Vasco UPV/EHU, P.O. Box 644, 48080 Bilbao, Spain. E-mail: benat.artetxe@ehu.eus, juanma.zorrilla@ehu.es*
[b]*BCMaterials Edificio Martina Casiano, 3rd Floor, UPV/EHU Science Park, Barrio Sarriena s/n, 48940 Leioa, Spain*
[c]*Institute for Advanced Materials and Mathematics (INAMAT²), Departamento de Ciencias, Universidad Pública de Navarra (UPNA), Campus de Arrosadia, 31006 Pamplona, Spain*
[d]*Servicios Generales de Investigación SGIker, Facultad de Ciencia y Tecnología, Universidad del País Vasco UPV/EHU, P.O. Box 644, 48080 Bilbao, Spain*
[e]*Cancer Heterogeneity Lab, Center for Cooperative Research in Biosciences (CIC bioGUNE), Basque Research and Technology Alliance (BRTA), Bizkaia Technology Park, 48160 Derio, Spain*

†Electronic supplementary information (ESI) available: Additional figures and experimental data related to the discussion of results. CCDC 2336816–2336818. For ESI and crystallographic data in CIF or other electronic format see DOI: https://doi.org/10.1039/d4dt00690a

lapse along the phase transition. In this context, polyoxometalates (POMs) are ideal candidates, because these well-known molecular metal-oxo clusters do not only provide structural stability, but can also confer their inherent properties (*e.g.* acidity, redox activity) on the system.[11] Examples of POM-based compounds already include those activated by light,[12] redox processes[13] and replacement of guest adsorbate molecules.[14] However, thermal activation and associated release of solvent molecules is the most common stimulus by far.[15]

Beyond the family of ionic crystals in which $[M_3O\{RCO_2\}_6L_3]^+$ macrocations ($M^{III}$ = Cr, Fe; L = terminal ligand) are combined with Keggin-type polyoxotungstates,[16,17] some of us opted for using copper(II) complexes of macrocyclic polyamines in combination with POM anions to construct hybrid compounds with the ability to undergo SCSC transformations. The available axial coordination sites, together with the plasticity of copper(II) ions and the ability of the macrocyclic ligands to establish weak but cooperative supramolecular interactions with oxygen-rich POM surfaces (*e.g.* hydrogen bonds, C–H···O type contacts) allows the construction of coordination networks while hindering the loss of crystallinity along the solid-state phase transition at the same time.

First, we prepared a family of hybrids made of Keggin-type anions and copper(II) complexes of bis(aminopyridil)-type ligands in which thermal dehydration induces reversible grafting of the metalorganic complexes to the POM surface or modifications on the conformation of the ligands.[18,19] Then, studies were extended to other $N_4$-chelating ligands, focusing our latest efforts on the $\{Cu(cyclam)\}^{2+}$ complex (cyclam = 1,4,8,11-tetraazacyclotetradecane) and addressing its ability to connect contiguous POM units through axial coordination in a series of covalent open frameworks.[20,21] When it comes to heteropolyoxometalate-based systems, we have reported (i) the transition from two-dimensional covalent assemblies to molecular hybrid species in a compound combining Keggin-type clusters with metal-cyclam complexes;[22] (ii) a full series of compounds formed by lanthanide-containing dimeric anions, which afford the coordinatively unsaturated species $[\{(\alpha\text{-}GeW_{11}O_{39})Ln(OAc)\}_2]^{12-}$ (Ln = La to Lu) upon dehydration;[23] and (iii) the B to A isomerisation of the well-known $[H_2As_2Mo_6O_{26}]^{4-}$ anion within a POM-metalorganic framework.[24] The latter constitutes one of the scarce literature examples of solid-state reactions involving major skeletal modifications of the metal-oxo cluster.[25] Taking a step forward, our very recent report on an extended hybrid framework able to undergo up to four sequential, thermally-triggered transformations that involve the rearrangement of octamolybdate anions into unprecedented isomeric forms through metal migration evidences that SCSC transformations can afford POM units that have not been isolated before by traditional synthetic procedures in solution.[26] Up to three different microporous phases with accessible voids were isolated from the parent hydrated phase, which exhibit robust water sorption properties.

All these results confirm that the ability of hybrid frameworks to undergo SCSC transformations is not limited to any specific type of POM anion. However, it is uncertain whether this behaviour can be extended to systems containing different metal complexes, beyond the examples based on $N_4$-type ligands. Thus, we decided to select picolinic acid (Hpic) as an example of planar, N,O-chelating aromatic ligand to be combined with copper(II) salts and Keggin-type anions in the quest of SCSC-displaying POM frameworks showing alternative metal complexes.[27] In the presence of guanidinium cations acting as structure-directing agents, the reaction with the copper(II)-monosubstituted Keggin-type phosphotungstate anion leads to the formation of the hybrid compound $[C(NH_2)_3]_{10}[\{PW_{11}O_{39}Cu(H_2O)\}_2\{Cu(pic)_2\}]\cdot 10H_2O$ (**1**). Thermal dehydration of **1** involves a structural rearrangement that proceeds *via* SCSC transformations to afford the anhydrous $[C(NH_2)_3]_{10}[\{PW_{11}O_{39}Cu\}_2\{Cu(pic)_2\}]$ (**2a**). This transformation implies the unprecedented solid-state polymerisation of the $\{PW_{11}O_{39}Cu\}$ cluster upon removal of its coordination water molecule. Compound **2a** reversibly adsorbs one water molecule per POM unit upon air exposure while retaining its single-crystallinity to afford the isostructural $[C(NH_2)_3]_{10}[\{PW_{11}O_{39}Cu\}_2\{Cu(pic)_2\}]\cdot 2H_2O$ (**2h**).

## Results and discussion

### Synthetic aspects

Motivated by the capacity of hybrid frameworks formed by the combination of POMs and $\{Cu(cyclam)\}^{2+}$ complexes to undergo SCSC transformations upon heating,[20–24] we undertook an analogous systematic exploration into the reactivity of the neutral $[Cu(pic)_2]$ complex prepared *in situ* with the Keggin-type $[PW_{12}O_{40}]^{3-}$ phosphotungstate anion. This planar, N,O-chelating aromatic ligand is expected to allow the axial coordination of $Cu^{II}$ centres to O atoms from POM surfaces and, simultaneously, to establish weak but cooperative π···π stacking interactions that may prevent structural collapse upon dehydration. Unfortunately, no hybrid framework was isolated from this set of reactions and most of them resulted in the co-crystallisation of both precursors. In a further effort, we decided to add guanidinium to the reaction mixtures before the crystallisation step because this cation has demonstrated a key role as structure-directing agent thanks to the extensive hydrogen bonding network that can establish with POM surfaces. Examples include its successful use as template of high-dimensional supramolecular frameworks,[28] as well as selective crystallising agent for diverse non-classical species, such as vanadates,[29] niobates,[30] metal-substituted POM assemblies,[31] giant molybdenum-blue rings[32] or organically derivatised clusters.[33,34] In these particular POM-bis(picolinate)copper(II) systems, our previous results[27] show that two isostructural $[C(NH_2)_3]_4[\{XW_{12}O_{40}\}\{Cu_2(pic)_4\}]\cdot[Cu_2(pic)_4(H_2O)]_2\cdot 6H_2O$ (X = Si, Ge) compounds can be isolated when using Keggin clusters with heteroatoms from group 14, which do undergo thermally-triggered, reversible SCSC transitions implying the splitting of $[Cu_2(pic)_4(H_2O)]$ dimeric complexes into $[Cu(pic)_2]$ monomers upon dehydration, while retaining the crystal packing almost

unaltered thanks to the preservation of the guanidinium-driven hydrogen-bonding network.

For POMs with heteroatoms of group 15, the reaction with the $[PW_{12}O_{40}]^{3-}$ anion in a 1 POM : 1 $Cu^{2+}$ : 2 pic molar ratio under synthetic conditions similar to those of the two compounds above (aqueous medium at pH *ca.* 4, room temperature) yielded blue crystals of **1** mixed with a colourless crystalline material after slow evaporation of the final solution. The former were separated manually under an optical microscope for a preliminary characterisation by FT-IR spectroscopy (Fig. S1†). Bands originating from $\nu_{as}$(P–$O_c$), $\nu_{as}$(W–$O_t$) and $\nu_{as}$(W–$O_b$–W) vibrational modes (O atoms: $O_c$ = central; $O_b$ = bridging; $O_t$ = terminal) were respectively observed at 1057, 956/885, and 812/748 $cm^{-1}$,[35] which, together with the presence of a Cu–O stretching signal at 696 $cm^{-1}$, revealed that the plenary POM precursor was transformed into the $[PW_{11}O_{39}Cu(H_2O)]^{5-}$ monosubstituted anion. The hybrid nature of **1** was confirmed by the additional bands found in the organic region above *ca.* 1100 $cm^{-1}$. In contrast to what observed for the compounds with $[XW_{12}O_{40}]^{4-}$ anions (X = Si, Ge), in which a monolacunary Keggin-type precursor transforms into a plenary cluster in the resulting hybrid compounds,[27] the $[PW_{12}O_{40}]^{3-}$ precursor undergoes partial hydrolysis and subsequent coordination to a copper(II) ion, evidencing that the nature of the heteroatom strongly influences the reactivity of Keggin anions.[11]

Following the observations above, a more rational synthetic approach to **1** was followed and the $[PW_{11}O_{39}]^{5-}$ precursor was reacted with a copper(II) salt and picolinic acid in a 2 : 3 : 2 stoichiometric molar ratio. Powder X-ray diffraction (PXRD) analyses showed that this combination afforded a pure sample of **1** (Fig. S2†) in *ca.* 10% yield, which was improved up to *ca.* 21% when the reaction was carried out at either 90 °C or reflux conditions. The effect of other synthetic parameters on the purity and the reaction yield was also evaluated, but none of them improved the results. These parameters are the molar ratios (1 : 1 : 1, 1 : 1 : 2 or 1 : 2 : 2), the amount of guanidinium added or the copper(II) source (nitrate, sulphate, chloride).

### Thermostructural behaviour

The thermal behaviour of **1** was investigated by a combination of thermogravimetric analyses (TGA) and variable-temperature PXRD experiments (VT-PXRD). The TGA curve (Fig. S3†) shows that the thermal decomposition of **1** occurs in three individual steps. The first stage originates from dehydration, which extends from room temperature to *ca.* 150 °C and accounts for a loss of 3.6% of the initial mass, corresponding to the evacuation of all of the crystallisation and coordination water molecules (calcd for 6 $H_2O$ molecules per POM: 3.3%). The second step reveals a thermal stability range that indicates the presence of a stable anhydrous phase up to *ca.* 270 °C. Above this temperature, the combustion of the organic ligands and the breakdown of the POM anion combine into the third stage, which leads to the final residue at *ca.* 630 °C. The mass of this residue is in good agreement with that expected for a mixture with a general formula $Cu_{1.5}O_{37}PW_{11}$ (exp. 83.5%; calcd 83.0%).

In order to determine whether **1** is able to maintain crystallinity or undergoes amorphisation along the thermal stability process, VT-PXRD experiments were performed from room temperature up to 530 °C (Fig. 1). The room-temperature diffraction pattern compares well with that calculated from single-crystal XRD (scXRD) data for **1**, which proves the homogeneity and purity of the crystalline phase (Fig. S4†). This initial phase is stable up to 50 °C as shown by the fact that no significant modifications are observed in neither the positions nor the intensities of the diffraction maxima. This temperature range spans near one third of the dehydration stage found in the TGA analyses and is followed by major changes in the diffraction patterns along the remaining two thirds to lead to a second thermally stable crystalline phase that corresponds to the anhydrous derivative **2a**. This phase can hardly be noticed at 130 °C when the region around $2\theta$ = 25° is inspected, but the transformation becomes completed at 170 °C, these temperatures being in accordance with that at which the stability range in the TGA curve starts. The four most intense maxima located at $2\theta$ = 8.0, 8.4, 9.1 and 9.5° in the pattern of **1** vanish and five new, well-defined maxima form at $2\theta$ = 8.2, 8.6, 9.0, 9.3 and 9.5° for **2a**. In addition, those appearing at $2\theta$ = 5.7° and 10.5° split into pairs at 6.3/6.8° and 10.2/10.6°, respectively, for **2a**. These observations indicate that: (i) four out of the five water molecules of hydration per POM are essential to maintain the crystal packing of **1** (mass loss at 50 °C: 0.70%; calcd for 1 $H_2O$ per POM: 0.55%); (ii) the fact that triggers SCSC transitions in **1** is the release of a second water molecule per POM; (iii) the transformation of **1** into **2a** is not a direct

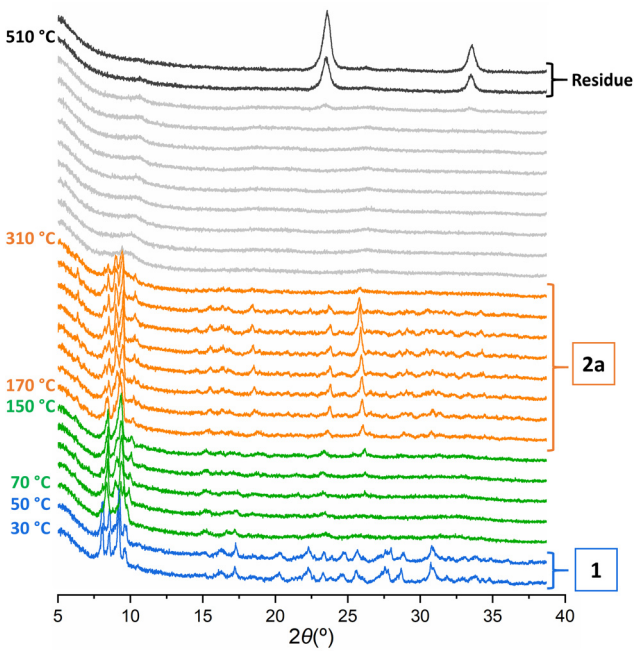


**Fig. 1** VT-PXRD patterns of **1** in the 30–530 °C temperature range.

process; (iv) the transition proceeds through most likely several intermediates of crystalline nature. Unfortunately, we were not able to determine the structure by scXRD of any intermediate corresponding to the 70–130 °C temperature range despite our several attempts. The anhydrous **2a** is stable up to 290 °C, loses crystallinity at 310 °C as shown by the substantial decrease in the diffraction intensity, and amorphises at temperatures above, which agrees with the third stage of decomposition in the TGA analyses. The final crystalline residue starts forming at 510 °C and has been identified at 650 °C as a mixture of monoclinic *Pmnb* $WO_3$ (PDF: 01-071-0131)[36] and monoclinic *C*2/*c* CuO (PDF: 00-002-1041)[37] in an approximate 7 : 1 ratio (Fig. S5†). We were unable to find any matching compound with phosphorus, which could be due to the formation of amorphous phosphorus oxide.

### Crystal structure of 1

Compound **1** crystallises in the monoclinic $P2_1/c$ space group, and its asymmetric unit contains one $[PW_{11}O_{39}Cu(H_2O)]^{5-}$ anion ($PW_{11}Cu$), one half of a $[Cu(pic)_2]$ metalorganic complex located in a special position, five guanidinium cations and a total of 5 hydration water molecules disordered over six crystallographic sites (Fig. S6†). The inorganic $PW_{11}Cu$ building block consists in the classical transition-metal monosubstituted α-Keggin-type structure, where the copper(II) atom is disordered over all the addenda metal positions, except for that connected to the metalorganic fragment. No preferential site is observed for the Cu atom because the population factors of the remaining eleven positions range all from 3 to 19% (Table S1†), and therefore, no significant lengthening of any $M{=}O_t$ bond is detected.

The metalorganic moiety is grafted at the POM surface and plays a bridging role between two contiguous clusters to lead to dimeric $[\{PW_{11}O_{39}Cu(H_2O)\}_2\{Cu(pic)_2\}]^{10-}$ molecular species (Fig. 2). Its metal centre displays a $\{CuN_2O_4\}$ chromophore in which the equatorial plane is defined by two N,O-chelating picolinate ligands in relative *trans* configuration [Cu–O = 1.945(5) Å and Cu–N = 1.951(7) Å], whereas terminal $O_{POM}$ atoms occupy the axial positions [$Cu{-}O_{POM}$ = 2.507(5) Å] (Table S2†). This arrangement results in an axially elongated octahedral geometry with a significant Jahn–Teller distortion. The crystal structure of **1** is formed by the $[\{PW_{11}O_{39}Cu(H_2O)\}_2\{Cu(pic)_2\}]^{10-}$ polyanions arranged in brick wall-like layers with a corrugation angle of 110° (Fig. 3 and S7†) that stack along the crystallographic [010] direction and within which the dimeric hybrid species are held together by a massive network of $O_w{-}H{\cdots}O_{POM}$, $N{-}H{\cdots}O_W$ and $N{-}H{\cdots}O_{POM}$ hydrogen bonds involving guanidinium cations and water molecules of hydration besides $O_{POM}$ atoms (Table S3†). This overall arrangement places Keggin clusters close to each other, showing intra- and inter-dimeric P⋯P distances of 14.715(4) and 12.5–12.8 Å, respectively.

### Thermally-triggered SCSC transformations

In view of the VT-PXRD results, we decided to explore whether the thermally-activated structural transformation of **1** could be

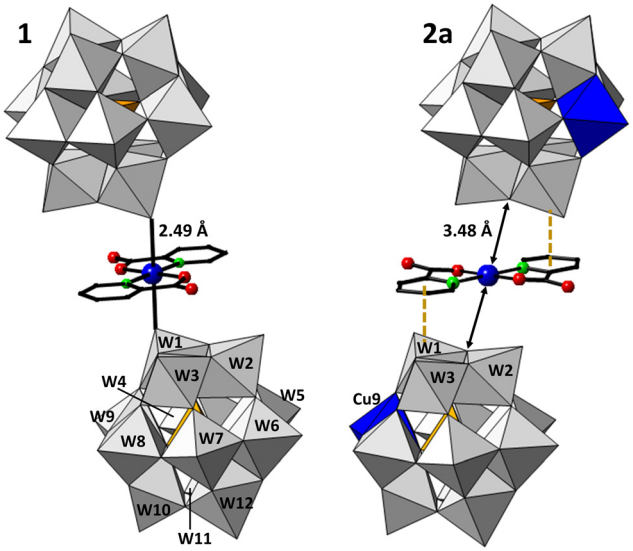


**Fig. 2** Comparison between the hybrid $[\{PW_{11}O_{39}Cu(H_2O)\}_2\{Cu(pic)_2\}]^{10-}$ dimer species in **1** and the supramolecular interaction between POMs and metalorganic complexes in **2a** originating from the cleavage of the coordination bond upon dehydration. Colour code: $WO_6$, grey octahedra; $PO_4$, orange tetrahedra; Cu, blue spheres; N, green spheres; O, red spheres; C, black sticks; π⋯trimer interactions in **2a** are depicted as dashed yellow lines. Note that the Keggin-type anion in **1** is depicted as a $[PW_{12}O_{40}]^{4-}$ plenary cluster due to the absence of preferential sites for the copper(II) centre within the inorganic POM skeleton.

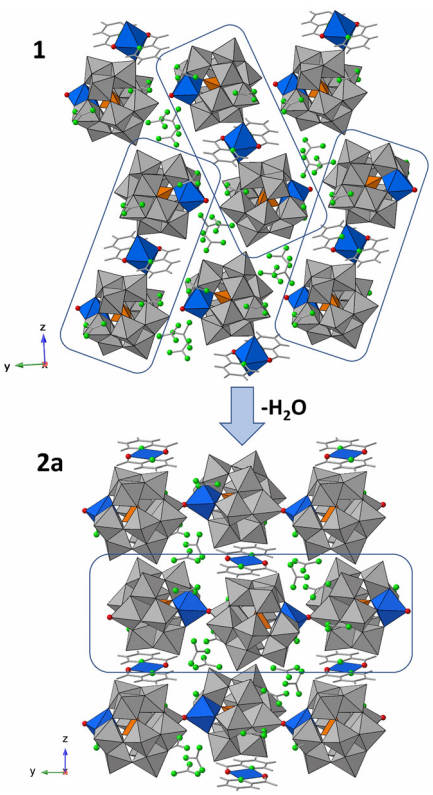


**Fig. 3** SCSC transformation in this work illustrated through the comparison between the crystal packing of **1** and **2a** viewed along the crystallographic *x* axis.

investigated by scXRD analyses. Thus, single crystals of **1** were heated to 170 °C in an oven to generate the anhydrous phase **2a** and quenched afterwards to 100 K in the diffractometer under a $N_2$ cryostream to perform a full data acquisition.

Phase **2a** also crystallises in the monoclinic $P2_1/c$ space group, but with significant modifications in the unit cell parameters upon dehydration. The *b* and *c* parameters respectively shorten in *ca*. 2.4 and 1.6 Å when going from **1** to **2a**, whereas *a* lengthens in *ca*. 1.0 Å. The new asymmetric unit is composed of one copper(II)-monosubstituted $[PW_{11}O_{39}Cu]^{5-}$ Keggin anion, one half of a $[Cu(pic)_2]$ complex located in a special position and five guanidinium cations acting as counterions (Fig. S6†).

The Keggin-type cluster loses the terminal aquo ligand from the copper(II) centre, but this atom retains its elongated octahedral geometry by coordinating to a terminal O atom of a POM subunit from a contiguous hybrid layer, which results in an unprecedented solid-state polymerisation of monosubstituted anions to lead to $\{PW_{11}Cu\}_n$ chains in **2a**. These modifications involve the rotation and subsequent re-orientation of all the Keggin type anions within the crystal packing, in such a way that the $Cu^{II}$ centre previously disordered over all of the addenda metal sites in **1** becomes preferentially located in positions 7 and 9 in *ca*. 45 : 55 ratio (Table S1†). This fact implies that corrugated $\{PW_{11}Cu\}_n$ chains with a corrugation angle of 123.5° run bidirectionally along the crystallographic *y* axis in the structure of **2a** (Fig. S8†). Several polymeric entities composed of monosubstituted Keggin anions connected through M–O–W corner-sharing linkages have been reported before,[35,38,39] but it is worth noting that most of them are linear despite the wide variety of heteroatoms (Si, Ge, P, As) and substituting metals (specially Co and Cu). To our knowledge, there are only few examples of corrugated chains with corrugation angles of about 120° and all of them have been accessed by hydrothermal methods.[39–42]

The solid-state polymerisation of $\{PW_{11}Cu\}$ units in this work is facilitated by the fact that Keggin anions get closer in *ca*. 1.5 Å along the crystallographic *y* axis when going from **1** to **2a** (P···P: 10.826(4) Å). This shift implies the cleavage of the Cu–O bonds in the metalorganic moiety, in such a way that the hybrid dimeric species in **1** are dismantled in **2a** and the $[Cu(pic)_2]$ units become interstitial square-planar complexes (Cu···O: 3.48(2) Å) embedded between fully inorganic guanidinium-$\{PW_{11}Cu\}_n$ layers in the crystallographic *xy* plane. Nevertheless, the complexes still interact closely with POM clusters from contiguous chains by establishing $O_{POM}\cdots\pi$ contacts between aromatic rings and $\{W_3O_{13}\}$ trimeric fragments (Fig. 2 and Table S3†). The crystal packing is stabilized by the massive network of $N–H\cdots O_{POM}$ hydrogen bonds established between guanidinium cations and POM surfaces (Fig. 3 and Table S4†). It is noteworthy that these contacts are more abundant in **2a** than in **1** despite the release of hydration water molecules that can act as both donors and acceptors. These weak but cooperative forces are most likely at the origin of this system undergoing thermal SCSC transitions, their presence being essential for this phenomenon to occur.

### Reversibility of the phase transition

The reversibility of the SCSC transformation was studied on crystalline samples of **2a** exposed to an open-air atmosphere for 1 and 7 days. TGA analyses revealed that **2a** only captures one water molecule per POM within the first 24 h (%*m*, found: 0.60), and that no additional molecules are adsorbed after 3 d of air exposure (%*m*, found: 0.78). Hydration–dehydration cycles in the resulting samples proved to be fully reversible (Fig. S9†), indicating that (i) dehydration of **1** into **2a** is irreversible, but (ii) a new phase (**2h**) is reversibly formed upon hydration of **2a**. These results are in good agreement with those from PXRD studies, which indicate that this new monohydrate phase **2h** is also crystalline with a structure different from that of the parent **1**. In fact, its diffraction pattern is virtually identical to that of **2a** except for the relative intensities of some diffraction maxima (Fig. S10†), which implies that minor differences should be expected between the crystal packing of **2a** and that of **2h**.

The scXRD experiments performed on crystals of **2a** exposed to open atmosphere revealed that the hydration from **2a** to **2h** proceeds *via* an additional SCSC transition. The cell parameters of **2h** are very similar to those of **2a** and the increase of the cell volume only accounts for 74 $Å^3$. Thus, the crystal packing is virtually identical with the adsorbed hydration water molecules playing no relevant structural role. These molecules locate next to the Cu–O–W linkages of the $\{PW_{11}Cu\}_n$ chains, interacting with adjacent POM units *via* hydrogen bonding (Fig. S11†).

### EPR spectroscopy

The phase transition from **1** to **2a** was monitored by X-band ($\nu$ = 9.39 GHz) and Q-band ($\nu$ = 33.90 GHz) electron paramagnetic resonance (EPR) spectroscopy performed from 4.2 K to room temperature on powdered samples. Room temperature spectra of **1** display complicated profiles with the overlapping of at least two signals originating from two different $Cu^{II}$ chromophores. The intense line at 11 670 Gauss in the Q-band spectrum (Fig. 4a), together with the partially resolved hyperfine structure represented as small signals at the low-field region, can be ascribed to a magnetically isolated $Cu^{II}$ ion in a regular octahedral geometry. The parallel component of the hyperfine structure resulting from the coupling of electronic ($S$ = 1/2) and nuclear spins ($I$ = 3/2) is also detected in the X-band spectrum as a group of four small shoulders located in the *ca*. 2650–2900 Gauss range. This signal was satisfactorily fitted (Fig. 4a) using an axial tensor with $g_{\|}$ = 2.436(1), $g_{\perp}$ = 2.096(1), $A_{\|}$ = 95(1) × $10^{-4}$ $cm^{-1}$, and $A_{\perp}$ < 28 × $10^{-4}$ $cm^{-1}$, thus corresponding to the $Cu^{II}$ centre located in the Keggin skeleton, in good agreement with literature fittings for similar systems.[38] In contrast, the second signal and hence, the full spectrum could not be coherently fitted in both bands. This discrepancy could *a priori* arise from a weak magnetic exchange that is strong enough to average the signals from magnetically non-equivalent centres in X-band ($E_{Zeeman}$ = 0.3 $cm^{-1}$), but too weak to do the same in the Q-band ($E_{Zeeman}$ = 1.1 $cm^{-1}$), at least in all directions. In fact, the spectrum remains virtually

 

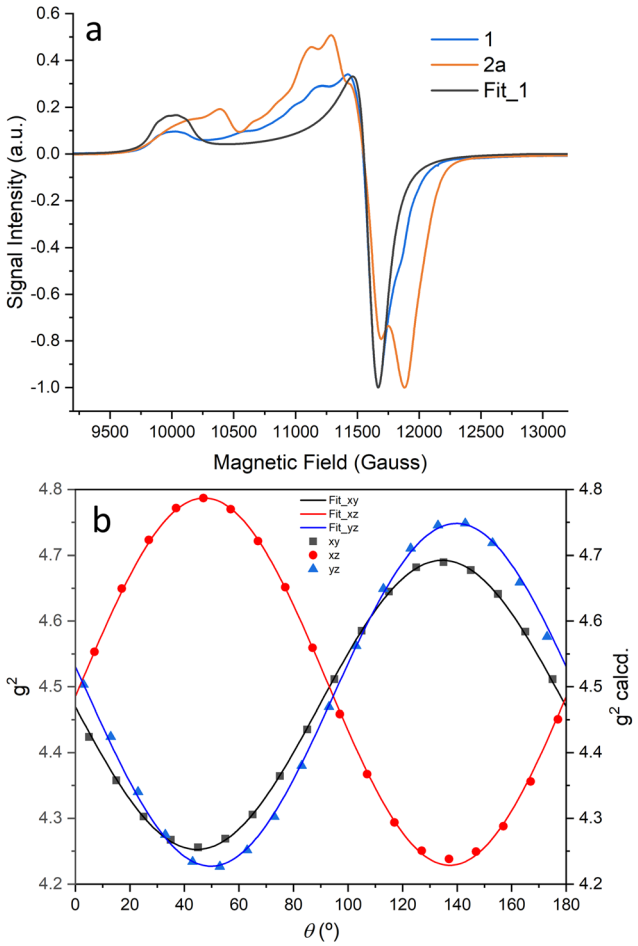


**Fig. 4** (a) Room temperature Q-band EPR spectra of **1** and **2a**, together with the partial fitting for **1** (see main text for details). (b) Angular dependence of the $g^2$-values in the X-band single-crystal EPR spectra for the three perpendicular planes. Experimental data is represented as symbols and calculated fittings as solid lines (see eqn (S1) in the ESI†).

unaltered upon lowering the temperature down to 4 K (Fig. S12†), which evidences that the magnitude of this magnetic coupling must be very small. Structurally, this would indicate that the $Cu^{II}$ centre in the octahedral $\{Cu(pic)_2O_2\}$ chromophore is not magnetically well-isolated and hence, the participation of the trimers that support such complex (with $Cu^{II}$ occupancies of *ca.* 5 and 8% in W2 and W3 addenda metal positions, respectively) in the exchange pathway cannot be disregarded.

To shed more light on this issue, we decided to carry out additional studies on single crystals of **1** by rotating them along three orthogonal orientations (Fig. S13†). All the X-band spectra show only one Lorentzian signal and no hyperfine structure, which implies that $Cu^{II}$ ions must be involved in a long-range magnetic system. Considering that the statistical disorder of the $Cu^{II}$ ion within the Keggin-skeleton would make it very difficult to observe its EPR signal in any crystallographic direction, the detected signal must be attributed to the centre in the metalorganic complex. The positions of the resonances were registered as a function of the orientation of the magnetic-field in the three planes studied (Fig. 4b). The least-squares fitting of the data (eqn (S1)†) allowed us to determine the main values of the *g* tensor: $g_1 = 2.235$; $g_2 = 2.061$; $g_3 = 2.055$. Even if these values corresponds to an exchange *g* tensor and do not directly reflect the molecular geometry of the chromophore, it can be noted that the smallest value of the *g* components appreciably deviates from $g = 2.0023$, in good agreement with a $d_{x^2-y^2}$ type ground state for a $Cu^{II}$ ion in an elongated octahedral geometry. The angular variations of the linewidths (Fig. S14†) are indicative of strong anisotropy in the magnetic interactions, which result in extremely narrow resonances in some particular orientations (linewidth <24 Gauss). This fact evidences that turning points could originate in powder patterns[43] and these would explain the additional shoulders that cannot be modelled with our two component systems.

In comparison to **1**, the spectra registered for **2a** at different temperatures (Fig. 4a and S12†) are even more complex and show (i) clear modifications in the relative intensities of the signals, in such a way that some of them are almost undetectable; and (ii) two additional signals located at *ca.* 10 470 and 11 360 Gauss in the Q-band spectra. However, the most noticeable difference consists in the virtual vanishing of the axial signal with hyperfine structure detected for **1** upon total dehydration. The structural rearrangement of Keggin anions along the phase transition and the preferential location of $Cu^{II}$ centres in the W7 and W9 addenda metal positions for **2a** favours the establishment of long-range magnetic interactions, which results in the subsequent collapse of the hyperfine structure.

### Electronic spectra

To evaluate whether the electronic properties of the title compounds vary along the transformation, we monitored the solid-state transition from **1** to **2a** through diffuse reflectance UV-Vis spectroscopy (DR-UV/Vis), because the insoluble nature of both compounds precluded us from performing solution studies. Blue crystals of **1** darken upon thermal dehydration to **2a**. This slight change in colour (inset – Fig. 5) already indicates that no major differences should be expected in the visible region of both spectra. The spectrum of **1** (Fig. 5) shows a group of three maxima with similar intensity at 787, 863 and 910 nm, together with a broad band centred at 620 nm. Structural transformation into **2a** decreases the intensity of the last two lines of the first group of signals, in such a way that the maximum at 787 nm becomes predominant. In addition, the band in the visible region is blue-shifted by 25 nm compared to that of **1**, which explains the colour change. In contrast, the two broad ligand-to-metal O → W charge transfer bands centred at 250 and 324 nm in the UV region of the spectra remain invariable along the phase transition.

## Experimental section

### Materials and methods

The precursor $K_7[\alpha\text{-}PW_{11}O_{39}]\cdot 14H_2O$ was synthesised following literature methods[44] and identified by FT-IR spectroscopy. All

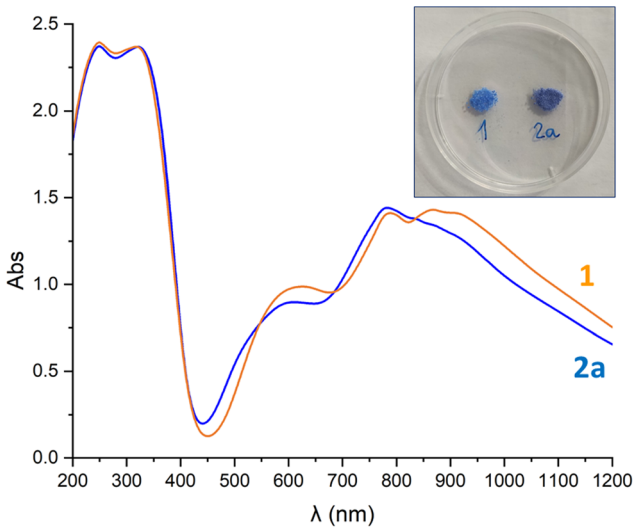


Fig. 5 Diffuse reflectance UV/Vis spectra of **1** and **2a**. Inset: photographs of crystalline samples.

other chemicals were obtained from commercial sources and used without further purification. The CHN content was determined on a PerkinElmer 2400 CHN elemental analyser using *ca.* 5 mg of powdered crystalline sample. FT-IR spectra were obtained as KBr pellets on a SHIMADZU FTIR-8400S spectrophotometer. The spectra were recorded with 4 $cm^{-1}$ resolution from 400 to 4000 $cm^{-1}$. TGA/DTA analyses were carried out from room temperature to 700 °C at a rate of 5 °C $min^{-1}$ on a Mettler Toledo TGA/SDTA851$^e$ thermobalance under a 50 $cm^3$ $min^{-1}$ flow of synthetic air. PXRD patterns were recorded in the $5 \leq 2\theta \leq 40°$ range (0.033° step size, 30 s per step) using a Philips X'PERT PRO diffractometer (40 kV/40 mA, $\theta$–$\theta$ configuration) equipped with monochromated CuKα radiation ($\lambda$ = 1.5418 Å) and a PIXcel detector. VT-PXRD patterns were collected on a Bruker D8 Advance diffractometer operating at 30 kV/20 mA and equipped with $CuK_\alpha$ radiation, a Vantec-1 PSD detector, an Anton Parr HTK2000 high-temperature furnace, and a Pt sample holder. Data sets were acquired from 30 to 750 °C every 20 °C, with a 0.16 °C $s^{-1}$ heating rate between temperatures. Theoretical powder diffraction patterns calculated from scXRD data were obtained using Mercury.[45] The reversibility of the structural transitions was studied by a combination of PXRD and TGA/DTA analyses using crystalline samples dehydrated to 200 °C at a 2 °C $min^{-1}$ rate under a 100 $cm^3$ $min^{-1}$ flow of synthetic air in a TA Instruments 2960 SDT thermobalance and left in contact with room moisture for different periods of time. EPR spectroscopy experiments were performed on different Bruker spectrometers: a Bruker ELEXSYS 500 spectrometer with a maximum available microwave power of 200 mW for the X-band measurements, which was equipped with a super-high-Q resonator ER-4123-SHQ and standard Oxford Instruments low temperature devices, and a Bruker EMX system for the Q-band studies, fitted in turn with an ER-510-QT resonator and an ER-4112-HV liquid helium cryostat. The magnetic field was calibrated by an NMR probe and the frequency inside the cavity was determined with a Hewlett-Packard 5352B microwave frequency counter. Powdered samples were placed in quartz tubes and spectra were recorded at different temperatures between 4 and 300 K using standard low temperature devices from Oxford Instruments. Single crystal studies on **1** were carried out by gluing a crystal of about 2.0 × 0.5 × 0.5 mm to a cleaved KCl cubic holder with its larger edge parallel to an edge of the KCl crystal. The sample holder was glued to an L-shaped quartz rod, and rotated with respect to the applied magnetic field using a manual Bruker goniometer. EPR spectra were recorded at room temperature rotating the crystal around the *X*, *Y* and *Z* axes, with 10° intervals along 180° in each plane. The spectra were adjusted using the WINEPR-Simfonia 1.5 simulation software (Bruker Analytische Messtechnik GmbH). Diffuse reflectance UV/Vis spectra were registered for crystalline samples using a double beam UV-Vis-NIR Agilent Cary 7000 spectrometer equipped with an integration sphere (Internal DRA 900).

### Synthesis of $[C(NH_2)_3]_{10}[\{PW_{11}O_{39}Cu(H_2O)\}_2\{Cu(pic)_2\}]\cdot 10H_2O$ (1), $[C(NH_2)_3]_{10}[\{PW_{11}O_{39}Cu\}_2\{Cu(pic)_2\}]$ (2a) and $[C(NH_2)_3]_{10}[\{PW_{11}O_{39}Cu\}_2\{Cu(pic)_2\}]\cdot 2H_2O$ (2h)

To a hot aqueous solution (20 mL) of $K_7[\alpha\text{-}PW_{11}O_{39}]\cdot 14H_2O$ (320 mg, 0.1 mmol), $CuCl_2\cdot 2H_2O$ (25 mg, 0.15 mmol) dissolved in 5 mL of water and picolinic acid (12 mg, 0.1 mmol) dissolved in 10 mL of water were successively added dropwise (pH ≈ 4) and the resulting blue reaction mixture was stirred at 90 °C for 1 h. After cooling down to room temperature and adding aqueous 1 M guanidinium chloride (1 mL), the final solution was left to slowly evaporate at room temperature and blue single crystals of **1** suitable for X-ray diffraction were obtained after 5 days. Yield: 20 mg (21% based on W). Anal. calcd for $C_{11}H_{46}Cu_{1.5}N_{16}O_{47}PW_{11}$ (%): C, 4.00; H, 1.40; N, 6.78. Found: C, 4.02; H, 1.42; N, 6.86. FT-IR (KBr, $cm^{-1}$): 3419 (w), 3352 (w), 3261 (w), 3189 (w), 2786 (w), 2688 (w), 1662 (vs), 1606 (s), 1567 (m), 1481 (w), 1456 (w), 1373 (m), 1295 (w), 1268 (w), 1099 (s), 1057 (s), 956 (vs), 885 (vs), 812 (vs), 748 (s), 696 (s), 594 (m), 515 (m), 407 (w). The anhydrous phase **2a** was obtained by heating crystals of **1** at 170 °C in an oven for 1 h, their colour subtly changing from light to dark blue upon dehydration. The hydrated phase **2h** was obtained after one day of exposure of **2a** to room atmosphere.

### Single-crystal X-ray crystallography

Crystallographic data for compounds **1**, **2a** and **2h** are provided in Table 1. Intensity data were collected at 100 K on a Rigaku Oxford Diffraction SuperNova diffractometer equipped with monochromated Mo Kα radiation ($\lambda$ = 0.71073 Å) and Eos CCD detector. For the data acquisition of **2a**, single crystals of **1** were heated in an oven to 443 K at a rate of 1 K $min^{-1}$ and kept at this temperature for 30 min to ensure full conversion. Immediately afterwards, the selected crystal was covered with Paratone® oil and placed under the $N_2$ stream of the diffractometer, the temperature of which was then set at 443 K to perform a preliminary unit cell determination. After confirming a unit cell different from that of **1** and a suitable diffracting

Table 1 Crystallographic data for compounds **1**, **2a**, and **2h**

| | **1** | **2a** | **2h** |
|---|---|---|---|
| Empirical formula | $C_{11}H_{46}Cu_{1.5}N_{16}O_{47}PW_{11}$ | $C_{11}H_{34}Cu_{1.5}N_{16}O_{41}PW_{11}$ | $C_{11}H_{36}Cu_{1.5}N_{16}O_{42}PW_{11}$ |
| Formula weight | 3303.27 | 3195.17 | 3213.19 |
| Crystal system | Monoclinic | Monoclinic | Monoclinic |
| Space group | $P2_1/c$ | $P2_1/c$ | $P2_1/c$ |
| $a$ (Å) | 11.96551(18) | 13.0736(3) | 13.1291(5) |
| $b$ (Å) | 21.5917(3) | 19.0786(6) | 19.1015(7) |
| $c$ (Å) | 22.2169(3) | 20.5732(7) | 20.7513(9) |
| $\beta$ (°) | 93.8906(14) | 93.780(3) | 93.490(4) |
| $V$ (Å$^3$) | 5726.65(15) | 5120.3(3) | 5194.5(4) |
| $Z$ | 4 | 4 | 4 |
| $\rho_{calc}$ (g cm$^{-3}$) | 3.831 | 4.145 | 4.109 |
| $\mu$ (mm$^{-1}$) | 22.685 | 25.356 | 24.996 |
| Collected reflections | 71 075 | 36 597 | 23 098 |
| Unique reflections ($R_{int}$) | 11 677 (0.042) | 10 054 (0.084) | 10 213 (0.060) |
| Observed reflections [$I > 2\sigma(I)$] | 10 170 | 7458 | 6861 |
| Parameters/restraints | 761/16 | 638/62 | 605/56 |
| $R(F)^a$ [$I > 2\sigma(I)$] | 0.028 | 0.074 | 0.087 |
| $wR(F^2)^b$ (all data) | 0.061 | 0.197 | 0.244 |
| GoF | 1.104 | 1.016 | 1.038 |

$^a R = \sum||F_o| - |F_c||/\sum|F_o|$. $^b wR^2 = [\sum w(F_o^2 - F_c^2)^2/\sum wF_o^2]^{1/2}$.

quality, the temperature was quenched to 100 K to proceed to the full data acquisition. In the case of **2h**, a single crystal of the anhydrous phase **2a** was exposed to room atmosphere for 24 h before the experiments. In all cases, data frames were processed (unit cell determination, intensity data integration, correction for Lorentz and polarization effects, and analytical absorption correction) using the CrysAlis software package.[46] The structures were solved using OLEX2 [47] and refined by full-matrix least-squares with SHELXL-2014/6.[48] Final geometrical calculations were carried out with PLATON[49] as integrated in WinGX.[50]

Thermal vibrations were treated anisotropically for heavy atoms (W, Cu, P) and O atoms belonging to the POM anions in all compounds, as well as for non-hydrogen atoms from picolinate ligands in **1** and **2a**. Hydrogen atoms of the picolinate ligands and guanidinium cations were placed in calculated positions and refined using a riding model with standard SHELXL parameters. For **1**, the $Cu^{II}$ atom of the Keggin subunit was disordered over all the addenda metal sites with terminal oxygen atoms not directly attached to any metalorganic complex. The $Cu^{II}$ occupancies were initially refined with no restrictions, leading to a total number of *ca.* one copper atom per Keggin. In the last refinement cycle, the sum of the copper population factors was restricted to 1.00. In contrast, this type of $Cu^{II}$ atom in **2a** and **2h** was found to be exclusively disordered over the two bridging positions W7 (45%) and W9 (55%) due to the solid-state polymerisation involving the condensation of $\{CuO_5\}$ and $\{WO_6\}$ fragments from contiguous Keggin subunits and subsequent rearrangement of the cluster orientations.

The structural disorder of some guanidinium cations was modelled by restricting the C–N (DFIX) and N–N (DANG) bond lengths to 1.33(2) and 2.20(2) Å, respectively. In the case of **2a** and **2h**, some isotropic thermal ellipsoids of the lighter atoms (C, N, O) were also normalised using SADI- and SIMU-type restraints from SHELXL. Regarding water molecules of hydration, six suitable positions were located in the Fourier map of **1** and their occupancies were initially refined without restrictions, resulting in a total number of 5.3 per Keggin subunit. The sum of population factors was fixed to 5.00 in the final refinement cycle in accordance with the results from TGA analyses. All of the structures show large maxima of residual electron density, which are located close to the W atoms according to the final difference density map. The existence of large residual maxima in the final Fourier map is a common fact in the refinement of polyoxotungstate-containing structures due to the high absorption of heavy atoms such as W.

## Conclusions

This work provides evidence of the fact that the ability of POM/metal–organic hybrid frameworks to undergo thermally-triggered single-crystal-to-single-crystal transformations is not limited to specific types of tetradentate, N-donor ligands. The reaction between neutral $[Cu(pic)_2]$ complexes (pic = picolinate) and copper(II)-monosubstituted Keggin-type phosphotungstate anions formed *in situ* led to the hybrid compound $[C(NH_2)_3]_{10}[\{PW_{11}O_{39}Cu(H_2O)\}_2\{Cu(pic)_2\}]\cdot 10H_2O$ (**1**) in the presence of structure-directing guanidinium cations. The extensive hydrogen bonding network established between cations and surface O atoms from the Keggin anions plays a key role in retaining the crystal integrity throughout the phase transition triggered by thermal dehydration in this system. Single-crystal X-ray diffraction demonstrates that the dimeric $[\{PW_{11}O_{39}Cu(H_2O)\}_2\{Cu(pic)_2\}]^{10-}$ molecular units in **1**, which are constituted by two Keggin type anions covalently linked through one octahedral $[Cu(pic)_2]$ complex, dismantle at 170 °C upon such

type of transition. Structural changes involve the cleavage and formation of Cu–O bonds, in such a way that $[Cu(pic)_2]$ moieties become square-planar interstitial complexes and unsaturated $\{PW_{11}O_{39}Cu\}$ units condense into $\{PW_{11}O_{39}Cu\}_n$ chains in an unprecedented solid-state polymerisation. This rearrangement implies the re-orientation and translation in *ca.* 1.5 Å of all the POM units. The transformation into the anhydrous $[C(NH_2)_3]_{10}[\{PW_{11}O_{39}Cu\}_2\{Cu(pic)_2\}]$ (**2a**) was found to be irreversible as confirmed by chemical and diffractometric analyses, which showed that it can only adsorb one water molecule per cluster to afford the hydrated $[C(NH_2)_3]_{10}[\{PW_{11}O_{39}Cu\}_2\{Cu(pic)_2\}]\cdot 2H_2O$ derivative (**2h**) without any significant alteration in its crystal structure. Potentially, compound **1** could be incorporated into a practical device that might serve as indicator to ensure that a given system does not exceed the temperature of 170 °C.

## Author contributions

E. R. B., S. R., and B. A. formal analysis, writing – original draft and review and editing; U. B., A. P., L. L. and L. S. F. investigation and data curation; M. M. V., J. M. G. Z. supervision, conceptualization and funding acquisition.

## Conflicts of interest

There are no conflicts to declare.

## Acknowledgements

This work has been funded by UPV/EHU (grant EHU-N23/03), Eusko Jaurlaritza/Gobierno Vasco (grants IT1722-22 and KK-2022/00045) and Ministerio de Ciencia e Innovación (PID2022-139530NB-I00). Technical and human support provided by SGIker (UPV/EHU, through ERDF and ESF) is gratefully acknowledged.

## References

1 J. J. Vittal, *Coord. Chem. Rev.*, 2007, **251**, 1781–1795.
2 F. F. Li, L. Zhang, L. L. Gong, C. S. Yan, H. Y. Gao and F. Luo, *Dalton Trans.*, 2017, **46**, 338–341.
3 X. Liang, S. Wang, J. Feng, Z. Xu, Z. Guo, H. Luo, F. Zhang, C. Wen, L. Feng, C. Wan and M.-M. Titirici, *Inorg. Chem. Front.*, 2023, **10**, 2961–2977.
4 M. Pisačić, I. Kodrin, N. Matijaković, N. Chatterjee, C. L. Oliver, B.-M. Kukovec and M. Đaković, *Cryst. Growth Des.*, 2020, **20**, 401–413.
5 Y. Jing, Y. Yoshida, T. Komatsu and H. Kitagawa, *Angew. Chem., Int. Ed.*, 2023, **62**, e202303778.
6 H. Ohwaki, N. Yoshinari and T. Konno, *Chem. Commun.*, 2019, **55**, 3402–3405.
7 J. Miao, Y. Nie, Z. Xiong, Y. Chai, S. Fu and H. Yan, *Dalton Trans.*, 2019, **48**, 5000–5006.
8 J.-P. Zhang, P.-Q. Liao, H.-L. Zhou, R.-B. Lin and X.-M. Chen, *Chem. Soc. Rev.*, 2014, **43**, 5789–5814.
9 P. Shen, W.-W. He, D.-Y. Du, H.-L. Jiang, S.-L. Li, Z.-L. Lang, Z.-M. Su, Q. Fu and Y.-Q. Lan, *Chem. Sci.*, 2014, **5**, 1368–1374.
10 M. Deng, S. Mukherjee, Y.-J. Liang, X.-D. Fang, A.-X. Zhu and M. J. Zaworotko, *Chem. Commun.*, 2022, **58**, 8218–8221.
11 M. T. Pope, *Heteropoly and IsopolyOxometalates*, Springer, Berlin, Germany, 1983.
12 J. Thiel, C. Ritchie, C. Streb, D.-L. Long and L. Cronin, *J. Am. Chem. Soc.*, 2009, **131**, 4180–4181.
13 L.-Z. Zhang, W. Gu, X. Liu, Z. Dong and B. Li, *CrystEngComm*, 2008, **10**, 652–654.
14 R. Eguchi, S. Uchida and N. Mizuno, *Angew. Chem., Int. Ed.*, 2012, **51**, 1635–1639.
15 S. Reinoso, B. Artetxe and J. M. Gutiérrez-Zorrilla, *Acta Crystallogr., Sect. C: Struct. Chem.*, 2018, **C74**, 1222–1242.
16 S. Uchida and N. Mizuno, *Coord. Chem. Rev.*, 2007, **251**, 2537–2546 and references therein.
17 Y. Shinoyama and S. Uchida, *Chem. Lett.*, 2021, **50**, 21–30.
18 A. Iturrospe, B. Artetxe, S. Reinoso, L. San Felices, P. Vitoria, L. Lezama and J. M. Gutiérrez-Zorrilla, *Inorg. Chem.*, 2013, **52**, 3084–3093.
19 A. Iturrospe, L. San Felices, S. Reinoso, B. Artetxe, L. Lezama and J. M. Gutiérrez-Zorrilla, *Cryst. Growth Des.*, 2014, **14**, 2318–2328.
20 J. Martín-Caballero, B. Artetxe, S. Reinoso, L. San Felices, O. Castillo, G. Beobide, J. L. Vilas and J. M. Gutiérrez-Zorrilla, *Chem. – Eur. J.*, 2019, **23**, 14962–14974.
21 J. Martín-Caballero, A. S. J. Wéry, S. Reinoso, B. Artetxe, L. San Felices, B. El Bakkali, G. Trautwein, J. Alcañiz-Monge, J. L. Vilas and J. M. Gutiérrez-Zorrilla, *Inorg. Chem.*, 2016, **55**, 4970–4979.
22 L. Fernández-Navarro, A. Iturrospe, S. Reinoso, B. Artetxe, E. Ruiz-Bilbao, L. San Felices and J. M. Gutiérrez-Zorrilla, *Cryst. Growth Des.*, 2020, **20**, 3499–3509.
23 J. Martín-Caballero, B. Artetxe, S. Reinoso, L. San Felices, P. Vitoria, A. Larrañaga, J. L. Vilas and J. M. Gutiérrez-Zorrilla, *Inorg. Chem.*, 2019, **58**, 4365–4375.
24 N. Dissem, B. Artetxe, L. San Felices, G. Beobide, O. Castillo, E. Ruiz-Bilbao, L. Lezama, M. dM. Vivanco, A. Haddad and J. M. Gutiérrez-Zorrilla, *Inorg. Chem.*, 2021, **60**, 14913–14923.
25 K. Uehara and N. Mizuno, *J. Am. Chem. Soc.*, 2011, **133**, 1622–1625.
26 E. Ruiz-Bilbao, A. Iturrospe, S. Reinoso, B. Artetxe, G. Beobide, L. San Felices, L. Lezama, J. M. Gutiérrez-Zorrilla, S. Darwish, D. Sensharma and M. J. Zaworotko, *Angew. Chem., Int. Ed.*, 2023, **62**, e202307436.
27 A. Pache, S. Reinoso, L. San Felices, A. Iturrospe, L. Lezama and J. M. Gutiérrez-Zorrilla, *Inorganics*, 2015, **3**, 194–218.
28 Y. Liu, C. Hu, A. Comotti and M. D. Ward, *Science*, 2011, **333**, 436–440.

 

29 R. Kato, A. Kobayashi and Y. Sasaki, *J. Am. Chem. Soc.*, 1980, **102**, 6571–6572.
30 S. Chen, P. Ma, H. Luo, Y. Wang, J. Niu and J. Wang, *Chem. Commun.*, 2017, **53**, 3709–3712.
31 M. Ibrahim, A. Haider, Y. Xiang, B. S. Bassil, A. M. Carey, L. Rullik, G. B. Jameson, F. Doungmene, I. M. Mbomekallé, P. de Oliveira, V. Mereacre, G. E. Kostakis, A. K. Powell and U. Kortz, *Inorg. Chem.*, 2015, **54**, 6136–6146.
32 A. Müller, L. Toma, H. Bögge, C. Schäffer and A. Stammler, *Angew. Chem., Int. Ed.*, 2005, **44**, 7757–7761.
33 Y. Zhang, M.-X. Li, Q. Hao, F. Su, Z.-M. Zhu, J.-S. Li, X.-J. Sang, C.-S. Wang and L.-C. Zhang, *Dalton Trans.*, 2020, **49**, 7234–7244.
34 L. F. Piedra-Garza, S. Reinoso, M. H. Dickman, M. M. Sanguineti and U. Kortz, *Dalton Trans.*, 2009, 6231–6234.
35 L. San Felices, P. Vitoria, J. M. Gutiérrez-Zorrilla, L. Lezama and S. Reinoso, *Inorg. Chem.*, 2006, **45**, 7748–7757.
36 E. Salje, *Acta Crystallogr., Sect. B: Struct. Crystallogr. Cryst. Chem.*, 1977, **33**, 574–577.
37 G. Tunell, E. Posnjak and C. J. Ksanda, *Z. Kristallogr. – Cryst. Mater.*, 1935, **90**, 120–142.
38 L. San Felices, P. Vitoria, J. M. Gutiérrez-Zorrilla, S. Reinoso, J. Etxebarria and L. Lezama, *Chem. – Eur. J.*, 2004, **10**, 5138–5146.
39 H. T. Evans Jr., T. J. R. Weakley and G. B. Jameson, *J. Chem. Soc., Dalton Trans.*, 1996, 2537–2540.
40 C. Wu, J. Lv, K. Yu, H. Zhang, C. Wang, C. Wang and B. Zhou, *J. Coord. Chem.*, 2017, **70**, 1862–1871.
41 L. Chen, F.-L. Jiang, N. Li, W.-T. Xu and M.-C. Hong, *J. Cluster Sci.*, 2008, **19**, 591–600.
42 J.-P. Wang, Y. Shen and J. Niu, *J. Coord. Chem.*, 2007, **60**, 1183–1190.
43 S. Ye, *Magn. Reson. Lett.*, 2023, **3**, 43–60.
44 R. Contant, W. G. Klemperer and O. Yaghi, *Inorg. Synth.*, 1990, **27**, 104–111.
45 C. F. Macrae, I. Sovago, S. J. Cottrell, P. T. A. Galek, P. McCabe, E. Pidcock, M. Platings, G. P. Shields, J. S. Stevens, M. Towler and P. A. Wood, *J. Appl. Crystallogr.*, 2020, **53**, 226–235.
46 *CrysAlisPro Software System, Version 171.40.67*, Agilent Technologies UK Ltd., Oxford, UK, 2012.
47 O. V. Dolomanov, L. J. Bourhis, R. J. Gildea, J. A. K. Howard and H. Puschmann, *J. Appl. Crystallogr.*, 2009, **42**, 339–341.
48 G. M. Sheldrick, *Acta Crystallogr., Sect. C: Struct. Chem.*, 2015, **71**, 3–8.
49 A. L. Spek, *Acta Crystallogr., Sect. D: Biol. Crystallogr.*, 2009, **65**, 148–155.
50 L. J. Farrugia, *J. Appl. Crystallogr.*, 2012, **45**, 849–854.